Applied Catalysis B: Environmental 125 (2012) 247–258

Contents lists available at SciVerse ScienceDirect

Applied Catalysis B: Environmental

journal homepage: www.elsevier.com/locate/apcatb

Novel, efficient and recyclable silica based organic–inorganic hybrid Nickel catalyst for degradation of dye pollutants in a newly designed chemical reactor

R.K. Sharma[a,*], Shikha Gulati[a], Amit Pandey[a], Alok Adholeya[b]

[a] Green Chemistry Network Centre, Department of Chemistry, University of Delhi, Delhi 110007, India
[b] Biotechnology and Management of Bioresources Division, The Energy and Resources Institute, Darbari Seth Block, India Habitat Centre, Lodhi Road, New Delhi 110003, India

ARTICLE INFO

Article history:
Received 20 April 2012
Received in revised form 22 May 2012
Accepted 30 May 2012
Available online 7 June 2012

Keywords:
Silica
Phthalocyanine
Recyclable catalyst
Azo dyes
Degradation

ABSTRACT

In this paper, a novel organic–inorganic hybrid heterogeneous catalyst was prepared through the immobilization of nickel tetrasulfophthalocyanine (NiTSPc) complex onto silica. The synthetic route is facile, cost effective and green. The catalyst was characterized by elemental analysis, diffuse reflectance UV–visible spectroscopy, ^{13}C CPMAS and ^{29}Si CPMAS NMR spectroscopy, X-ray diffraction (XRD), Scanning electron microscopy (SEM), BET surface area analysis, Energy dispersive X-ray fluorescence (ED-XRF) and Fourier transform Infrared (FT-IR) spectroscopic techniques. The catalytic performance of the novel organic–inorganic hybrid catalyst was evaluated in the oxidative degradation of azo dyes at room temperature using hydrogen peroxide as an environmentally benign oxidant. The conditions for maximum dye degradation were optimized in terms of catalyst loading, H_2O_2 dosage and initial pH of the solution. The dye degradation followed pseudo first order kinetics. GC–MS was used to analyze the products formed after the dye degradation. The hybrid catalyst showed up to 96% of degradation efficiency, and can be recovered and reused for multiple cycles without appreciable loss in its catalytic activity. In addition, a novel chemical reactor with automated modes has been designed for the first time which opens up a new avenue for the effective and large scale degradation of dyes at room temperature using recyclable organic-inorganic hybrid catalyst.

1. Introduction

Azo dyes constitute the most versatile class of commercial dyes, and are widely used in the textiles, cosmetics, plastics, leather, food colorants, printing and pharmaceutical industries [1]. Consequently, the effluents from these industries consist of large quantities of dye ingredients which have a strong detrimental impact on human health as well as on the environment due to their toxic, non-biodegradable and mutagenic properties [2–4]. Thus, the adversity of these dyes even at trace level attracts the scientists to develop efficient processes for their degradation. Various methodologies like adsorption methods, biological degradation, coagulation processes, ozonation, Fenton's reagent method, hypochlorite treatment, etc. have been extensively employed for the removal of these dyestuffs [5–10]. In recent years, with growing concerns for the conservation of ecosystem, new technologies have been developed for more efficient treatment of industrial effluents. Among them, Advanced Oxidation Processes (AOPs) using catalysts appear to be a promising technology for the destruction of target pollutants [11]. Taking into consideration the degradation of azo dyes, AOPs using eco-friendly oxidant, i.e. hydrogen peroxide represents a significant approach to destroy the chromophoric system of these dyes, and accomplish high mineralization degree.

Metallophthalocyanines have engrossed noteworthy attention for their catalytic applications particularly in the treatment of pollutants owing to their facile preparation, excellent thermal stability, economic viability and high catalytic activity [12–14]. However, many homogeneous metallophthalocyanine catalysts have shown low activity because of their tendency to form inactive aggregates in solution. Moreover, these homogeneous catalysts are difficult to separate from the reaction media. To overcome these disadvantages, immobilization of metallophthalocyanines onto solid support materials has been carried out, where the catalytic site was protected [15–19]. The immobilization of the catalytic centre on support materials with large specific surface areas presents numerous advantages in comparison to their soluble counterparts such as easy separation by filtration, robustness, high stability, potential recyclability, and provides more catalytic active centers. There are various porous support materials available on which metal complexes have been immobilized. Among them, silica gel is very advantageous since it possesses high surface area, good thermal and mechanical stability, easy availability, economic viability, and relatively simple and robust covalent modification with organic or organometallic moieties [20].

* Corresponding author. Tel.: +91 011 27666250; fax: +91 011 27666250.
E-mail address: rksharmagreenchem@hotmail.com (R.K. Sharma).

0926-3373/$ – see front matter © 2012 Elsevier B.V. All rights reserved.
http://dx.doi.org/10.1016/j.apcatb.2012.05.046

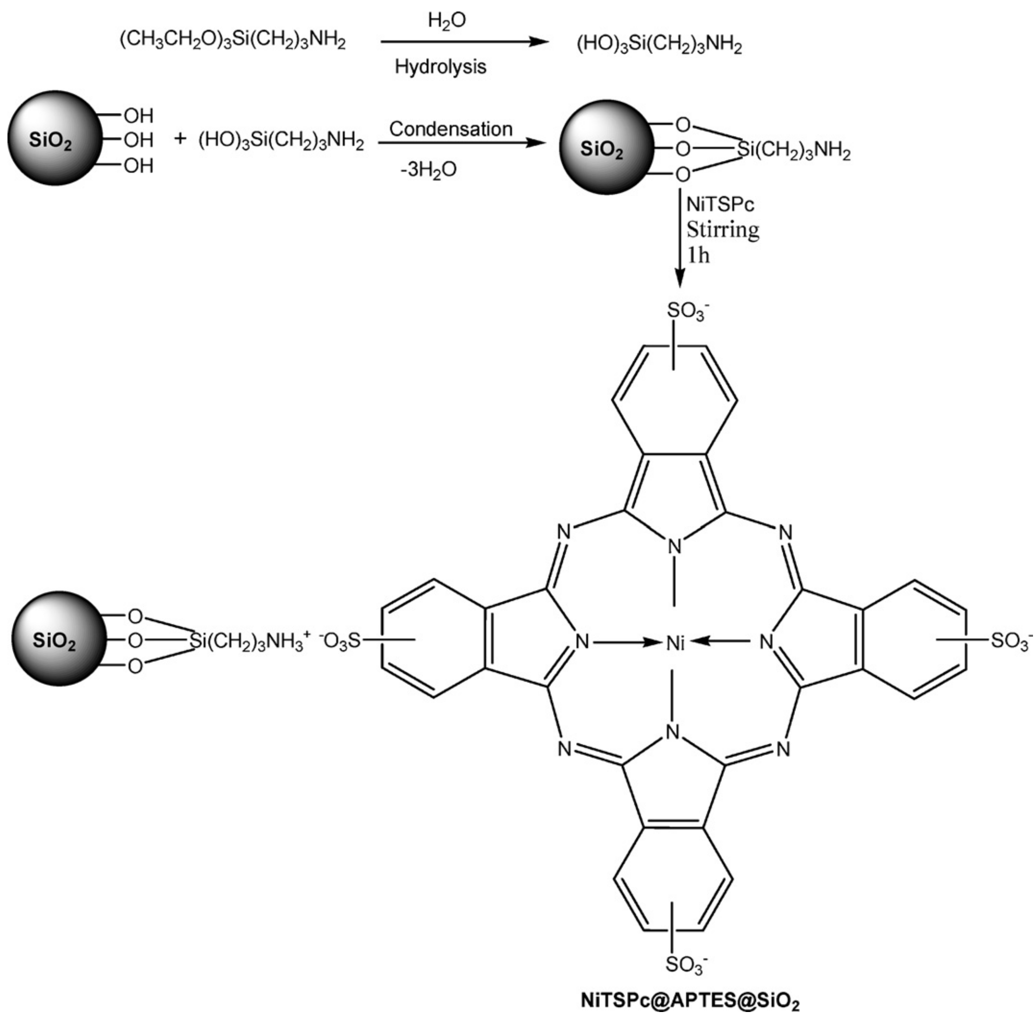

Scheme 1. Preparation of silica-supported Nickel catalyst (NiTSPc@APTES@SiO_2).

The aim of this study is to explore a novel catalyst, i.e. Silica supported Nickel(II) tetrasulfophthalocyanine catalyst (NiTSPc@APTES@SiO_2), which overcomes the traditional drawbacks of homogeneous catalyst and has a good prospect for its broad application. Recently, we have developed Cu^{2+}-perfluorophthalocyanine-immobilized silica gel catalyst for the oxidative bromination reaction under mild reaction conditions [21]. Thus, in continuation of our work on the synthesis of organic–inorganic hybrid materials, and their applications as metal scavengers, sensors, and catalysts for various organic transformations [22–28], herein we report the synthesis, characterization and application of silica supported Nickel(II) tetrasulfophthalocyanine catalyst for the oxidative degradation of azo dyes at room temperature using hydrogen peroxide as an environmentally benign oxidant.

2. Experimental

2.1. Materials and reagents

3-Aminopropyltriethoxy silane, APTES (98%), silica gel (60–100 mesh, according to the supplier specifications), Nickel tetrasulfophthalocyanine (NiTSPc), H_2O_2 solution (30 wt% in water) and Methyl Orange were purchased from Sigma–Aldrich. All other dyes were commercial compounds and were used without further purification. Other chemicals used were of analytical reagent grade and were used as received without further purification. Double distilled water was used throughout this study.

2.2. Catalyst preparation

2.2.1. Functionalization of silica gel (SiO_2) with APTES

SiO_2 was functionalized using APTES to yield aminopropyl-functionalized silica gel (APTES@SiO_2) according to a greener protocol (Scheme 1) [29]. Prior to the functionalization procedure, the silica gel was dried in vacuum oven at 150 °C to remove any physisorbed water. Afterwards, 1 mL of APTES was dissolved in 100 mL of distilled water acidified with acetic acid (pH 4). Then, 2 g of activated silica gel was added in the silane solution and stirred for 2 h at room temperature. The resulting material (APTES@SiO_2) was filtered off and kept in oven at 150 °C for 4 h. The dried product was washed consecutively with water, ethanol and acetone several times to remove the un-grafted material and dried for another 2 h at 120 °C.

2.2.2. Immobilization of NiTSPc complex onto APTES@SiO_2

The covalent grafting of NiTSPc complex on APTES@SiO_2 was carried out to yield Nickel tetrasulfophthalocyanine functionalized silica gel (NiTSPc@APTES@SiO_2). A mixture of APTES@SiO_2 (5 g) and NiTSPc (0.5 mmol) solution in water was stirred at room temperature for 2 h. The buffer solution (NH_4OH-NH_4Cl) maintained the pH of the solution at 10. After that, the material was filtered, washed

with water and dried in vacuum oven to give a blue solid material, NiTSPc@APTES@SiO_2 (Scheme 1).

2.3. Catalytic reaction procedure

The catalytic reactions were carried out in a 50 mL round-bottomed flask. All reactions were performed in neutral aqueous solutions. The typical reaction mixture contained the 25 mL dye solution (3×10^{-5} M), NiTSPc@APTES@SiO_2 catalyst (0.02 g) and H_2O_2 (17.6 mmol, 2 mL). The reaction flask was agitated in a rotary mechanical shaker at room temperature. Samples of the reaction mixture were withdrawn at regular intervals and analyzed on a UV–visible spectrophotometer. The catalyst was separated from the reaction mixture by simple filtration. Absorbance measurements were recorded in the range of 200–800 nm, and the maximum absorption wavelength (λ_{max} = 462 nm) for the dye (Methyl Orange) was used for the calibration curves and further concentration measurements. The degradation efficiency catalyzed by NiTSPc@APTES@SiO_2 was evaluated by the degradation ratio of Methyl Orange which was calculated with the following formula: $[(C_0 - C_t)/C_0] \times 100$; where C_t and C_0 represent the time-dependent concentration and the initial concentration, respectively.

2.4. Product analysis and identification using GC–MS

GC–MS analysis was performed using Agilent gas chromatography (6850 GC) with a HP-5MS 5% phenyl methyl siloxane capillary column (30.0 m × 250 μm × 0.25 μm) and a quadrupole mass filter equipped 5975 mass selective detector (MSD) for the analysis of the degradation products. The carrier gas was helium (rate 0.9 ml min^{-1}) and the temperature of the injection port was 250 °C. The temperature program of the column was set to an initial oven temperature of 60 °C and was increased at a rate of 10 °C/min to 250 °C, and the oven was held at 250 °C for 10 min. The sample for GC–MS analysis was prepared as follows: after the degradation reaction of Methyl Orange, the aqueous solution was withdrawn, and the water was removed under vacuum. The residue obtained was dissolved in hydrochloric acid (2 M), and the resulting solution was saturated with sodium chloride and was extracted with diethyl ether. The combined ether extracts were dried over anhydrous sodium sulfate, and the ether was evaporated under vacuum. The residue was then dissolved in methanol solution before GC–MS analysis.

2.5. Physico-chemical characterizations

Specific surface area was calculated using the BET method on Gemini-V2.00 instrument (Micromeritics Instrument Corp.). Samples were outgassed at 100 °C for 3 h to evacuate the physically adsorbed moisture before measurement. Solid-state ^{13}C and ^{29}Si cross-polarization magic-angle spinning (CPMAS) NMR spectra were recorded on Bruker DSX-300 NMR spectrometer. The Fourier transform infrared (FTIR) spectra of the compounds were obtained on a Perkin-Elmer spectrometer at room temperature using KBr pellet technique in the range of 4000–400 cm^{-1} under the atmospheric conditions with a resolution of 1 cm^{-1}. All samples and KBr were dried at 100 °C overnight before KBr pellets preparation. The diffuse reflectance UV–visible spectrum of the catalyst was obtained over the spectral range 300–800 nm in the $BaSO_4$ phase using Perkin Elmer Lambda 35 scanning double beam spectrometer equipped with a 50 mm integrating sphere. Elemental analysis (CHN) was performed using Elementar Analysensysteme GmbH VarioEL V3.00 instrument. Energy dispersive X-ray fluorescence spectroscopy was performed on Fischerscope X-Ray XAN-FAD BC. XRF spectrometer was equipped with a tungsten anode. Excitation X-ray beam was pre-treated by collimator (0.6 Dm) and Ni filter. The tube was operated at 50 kV and 850 μA. The spectrum collection live time was 36 s per sample. The instrument control, signal acquisition, spectrum handling and quantitative analysis were carried out using WinFTM® Software. The color video camera was used for accurate selection of analyzed part of the sample. LABINDIA AA 7000 Atomic Absorption Spectrometer was used to test the leaching of the catalyst. Scanning electron microscopy (SEM) images were obtained using a ZEISS EVO 40 instrument. The samples were placed on a carbon tape and then coated with a thin layer of gold using a sputter coater. Powder X-ray diffraction (XRD) patterns of the samples were obtained on a Bruker D8 ADVANCE X-ray diffractometer using graphite monochromatized Cu–Kα radiation. The UV–vis spectra were recorded using Double beam UV–visible spectrophotometer of UV 5704M Electronics Corporation of India Limited.

3. Results and discussion

3.1. Influence of pH in the preparation of catalyst

A NiTSPc stock solution (50×10^{-6} M) was prepared by dissolving 0.05 g of NiTSPc in 1000 mL of distilled water. The appropriate buffer solutions were used in order to maintain the pH of the NiTSPc solutions. The Q-band in the electronic absorption spectrum, which is attributed to a π–π* transition in the phthalocyanine ring, depends on the environment of the solution. Therefore, the UV–visible spectrum of NiTSPc exhibits two peaks in the Q-band region due to its tendency to exist in monomeric as well as in dimeric species in aqueous solution [30]. The band near 618 nm is associated with the monomeric species, and the band near 597 nm is assigned to the dimeric species. Generally, hydrophobic π systems aggregate in polar solvents (such as water) [31]. Therefore, the effect of initial pH of the solution on aggregation was investigated. The UV–visible spectra of NiTSPc aqueous solutions were obtained in the pH range of 2–12 and are shown in Fig. 1. It is clearly seen that the intensity of peak due to monomeric species increased up to pH 10 while that of dimeric species decreased. These results suggest that catalyst could be prepared at a pH of 10 as abundant NiTSPc monomers are formed in alkaline solution. Hence, the better catalytic activity of NiTSPc could be accomplished by immobilizing catalyst monomers onto APTES@SiO_2 to give NiTSPc@APTES@SiO_2.

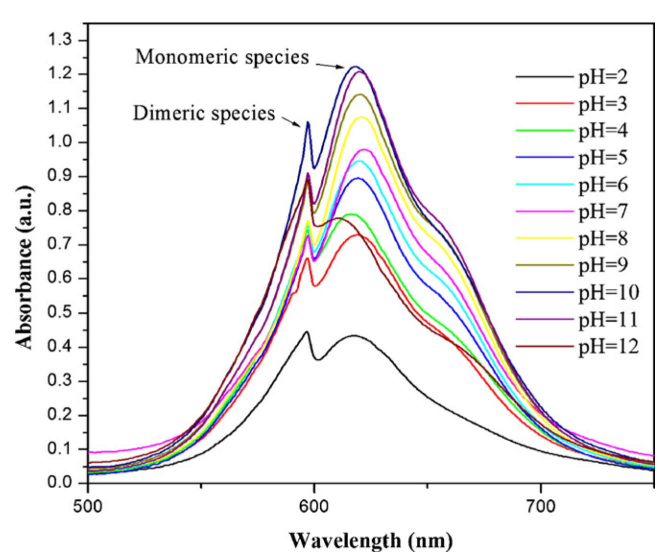

Fig. 1. UV–visible spectra of NiTSPc aqueous solutions under different pH conditions.

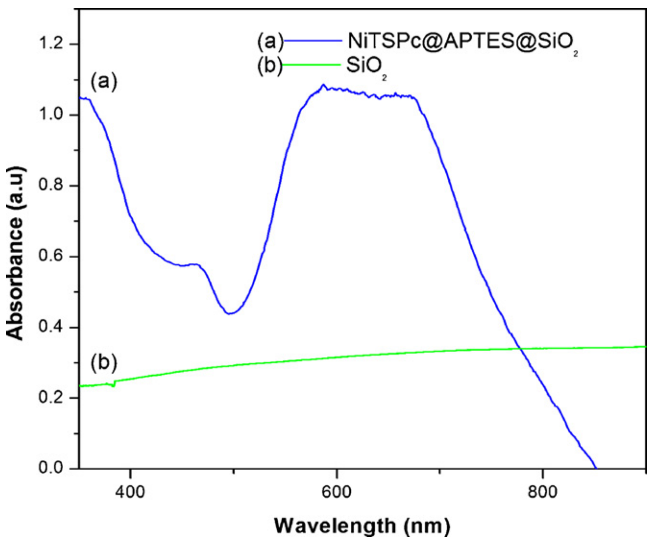

Fig. 2. Diffuse reflectance UV–visible spectra of (a) NiTSPc@APTES@SiO_2 and (b) SiO_2.

3.2. Catalyst characterizations

3.2.1. Diffuse reflectance UV–visible spectroscopy

The diffuse reflectance UV–visible spectra of SiO_2 and NiTSPc@APTES@SiO_2 are shown in Fig. 2. The spectrum of SiO_2 does not have any absorption band in the region of 400–900 nm. On the other hand, the diffuse reflectance UV–visible spectrum of NiTSPc@APTES@SiO_2 exhibits broad absorption band in the region of 550–800 nm due to ligand π–π^* electronic transitions which is comparable to those of the un-grafted complex (λ_{max} = 657 nm) [3], confirming that NiTSPc complex has been covalently anchored on silica surface without degradation. The blue shift was also observed, indicating better π overlap on immobilization of the NiTSPc complex [32].

3.2.2. Solid state ^{13}C CPMAS and ^{19}Si CPMAS NMR spectroscopy

The presence of 3-aminopropyl group after functionalization of SiO_2 with APTES is confirmed by solid state ^{13}C CPMAS NMR spectroscopy. The ^{13}C NMR spectrum of APTES@SiO_2 (Fig. 3a) shows the presence of three well resolved peaks at 9.44, 20.99 and 42.68 ppm assigned to the carbons of the incorporated aminopropyl group which authenticate the synthesis of APTES@SiO_2 [33]. The covalent linkage between the silanol groups and the organic moiety on the silica can also be monitored by means of ^{29}Si CPMAS NMR spectroscopy. The solid-state ^{29}Si NMR spectrum (Fig. 3b) of NiTSPc@APTES@SiO_2 shows peaks at −58 ppm and −67 ppm assigned to Si—OH of C—$Si(OSi)_2(OH)$ group (T^2) and C—$Si(OSi)_3$ group (T^3) respectively, which provides clear evidence that the hybrid NiTSPc@APTES@SiO_2 sample consists of a highly condensed siloxane network with an organic group covalently bonded to SiO_2. Two other typical peaks correspond to the inorganic polymeric structure of silica: −111 ppm assigned to $Si(OSi)_4$ group (Q^4) and −101 ppm assigned to the free silanol group of $Si(OSi)_3OH$ (Q^3) [34,35].

3.2.3. Energy dispersive X-ray fluorescence spectroscopy

The conventional methods (AAS, ICP-MS) of metal analysis requiring sample in the form of solution suffer from various drawbacks like use of highly corrosive chemicals (HNO_3, HCl, aqua regia, HF) for the preparation of sample, and also sample consumption is often inadequate for these procedures. Energy dispersive X-ray fluorescence (ED-XRF) is an attractive and non-destructive technique that is environmentally friendly because it minimizes the number of sample preparation steps and, therefore, the waste generated. The analytical methods involving ED-XRF do not require the sample to be subjected to any drastic treatment, such as use of concentrated acids, delayed heating, etc. Therefore, metal loading in the silica supported catalyst (NiTSPc@APTES@SiO_2) was determined by ED-XRF. Samples were pressed as homogeneous tablets of the compressed powder of the catalytic system. Fig. 4 presents a typical ED-XRF spectrum of a supported catalyst system (NiTSPc@APTES@SiO_2). In the measured region, we can observe the presence of well-resolved Kα line of Ni atoms, and thus the nickel content (4.1%, w/w) was determined directly in NiTSPc@APTES@SiO_2 avoiding digestion step as in the case of absorption or emission atomic spectroscopy techniques.

3.2.4. Fourier-transform Infrared spectroscopy

The silica-based materials are characterized by FT-IR spectroscopy. The spectra of SiO_2, APTES@SiO_2 and NiTSPc@APTES@SiO_2 shown in Fig. 5 exhibits the characteristic bands of the silica framework related to Si—O—Si asymmetric stretching (1087 cm^{-1}), Si—O stretching of Si—OH and Si—O^- groups on the surface (965 cm^{-1}), Si—O—Si symmetric stretching (800 cm^{-1}) and Si—O—Si bending vibrations (467 cm^{-1}) [36,37]. Additionally, the spectrum presents a band at 1645 cm^{-1} associated with H—O—H bending vibrations of physically adsorbed water and a broad band centered around 3460 cm^{-1} due to O—H stretching vibrations of hydrogen-bonded surface silanol groups and physically adsorbed water (supplementary information). The post-grafting of APTES onto SiO_2 is confirmed by the appearance of new peak at 2925 cm^{-1}, which is due to the C—H stretching of the functionalized aminopropyl group (which does not appear in the parent SiO_2 spectrum). Also, the peak due to silanol groups present in SiO_2 has disappeared in APTES@SiO_2. This is because of the reaction between the surface Si—OH groups of SiO_2 and ethoxy groups of APTES during the modification reaction. Furthermore, moving from SiO_2 to APTES@SiO_2, significant reduction of the intensity of the O—H stretching and bending vibrations bands and of the peak from Si—OH stretching modes is observed. The peak around 1645 cm^{-1} corresponds to N—H bending vibration of —NH_2 groups, which is overlapped by the bending vibration of adsorbed H_2O. The IR bands related to the anchored complex are very weak when compared to those associated with the support and grafted APTES, due to the low complex loading and also because of the superimposition of characteristics peaks of NiTSPc (Fig. 5d) by a broad polymer band around 1087 cm^{-1} [38]. By comparing the spectra of APTES@SiO_2 with those of NiTSPc@APTES@SiO_2, it is observed that the absorption at 1645 cm^{-1} is shifted to 1647 cm^{-1} and also the intensity of this peak has decreased after immobilization confirming that NiTSPc is successfully anchored onto the surface of SiO_2.

3.2.5. Surface area and elemental analysis

A high-quality distribution of catalytic active species over a high surface area support material is usually enviable for superior catalytic activity. Generally, the anchoring of organic or organometallic moieties onto the silica matrix blocks the access of nitrogen gas molecules thereby reduces its surface area. Hence, as estimated, the BET surface area decreased after grafting [39–41], according to the following sequence SiO_2 > APTES@SiO_2 > NiTSPc@APTES@SiO_2. The reduction in surface area in this sequence confirms the functionalization of silica gel with 3-aminopropyltriethoxy silane to give APTES@SiO_2, and its further modification with NiTSPc to yield NiTSPc@APTES@SiO_2. The results are presented in Table 1. The ninhydrin test was performed to detect qualitatively the existence of free amine species on APTES@SiO_2 (Supplementary information) [42]. The color of the material changed from white to blue when the ninhydrin solution

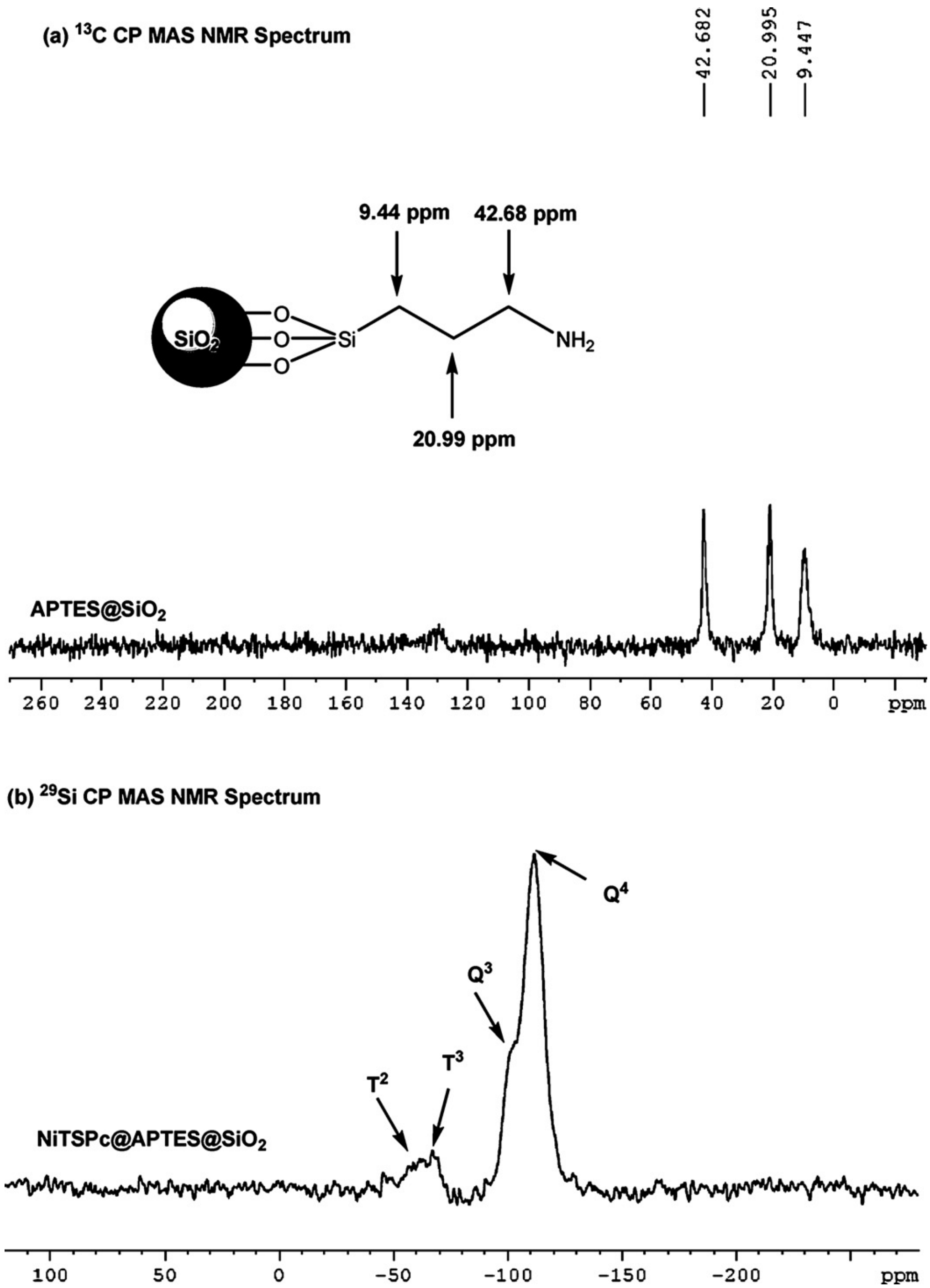

Fig. 3. (a) ^{13}C CPMAS NMR spectrum of APTES@SiO_2 and (b) ^{19}Si CPMAS NMR spectrum of NiTSPc@APTES@SiO_2.

was added, confirming the presence of free amine groups. In contrast, the test was negative for the parent SiO_2 (no color change). The elemental analysis of APTES@SiO_2 leads to the appearance of nitrogen (1.21%) as well as the carbon surface content (3.26%), providing a first evidence for the APTES immobilization onto SiO_2. The observed carbon and nitrogen contents of APTES@SiO_2 shows C/N ratio to be ∼2.6 which is close to the expected value thereby confirming the APTES grafting onto the surface of SiO_2. The nitrogen loading of APTES@SiO_2 was found to be 0.86 mmol g^{-1}. The chemical analyses of NiTSPc@APTES@SiO_2 revealed the presence of organic matter with a C/N ratio roughly similar to that of phthalocyanine.

3.2.6. X-ray diffraction studies

X-ray diffraction (XRD) analysis is carried out to investigate the structural characteristics of SiO_2, APTES@SiO_2 and NiTSPc@APTES@SiO_2. The diffractograms of these materials presented in Fig. 6 shows that all these materials are amorphous or non-periodic. The broad peak centered around $2\theta = 23^\circ$ in the XRD patterns of SiO_2, APTES@SiO_2 and NiTSPc@APTES@SiO_2 is ascribed to the diffraction peak of amorphous silica, which clearly depicts that there is no change in the topological structure of SiO_2 before and after grafting reactions [43]. However, after organo-functionalization and metal complex loading there is a slight decrease in intensity [44] with broadening of

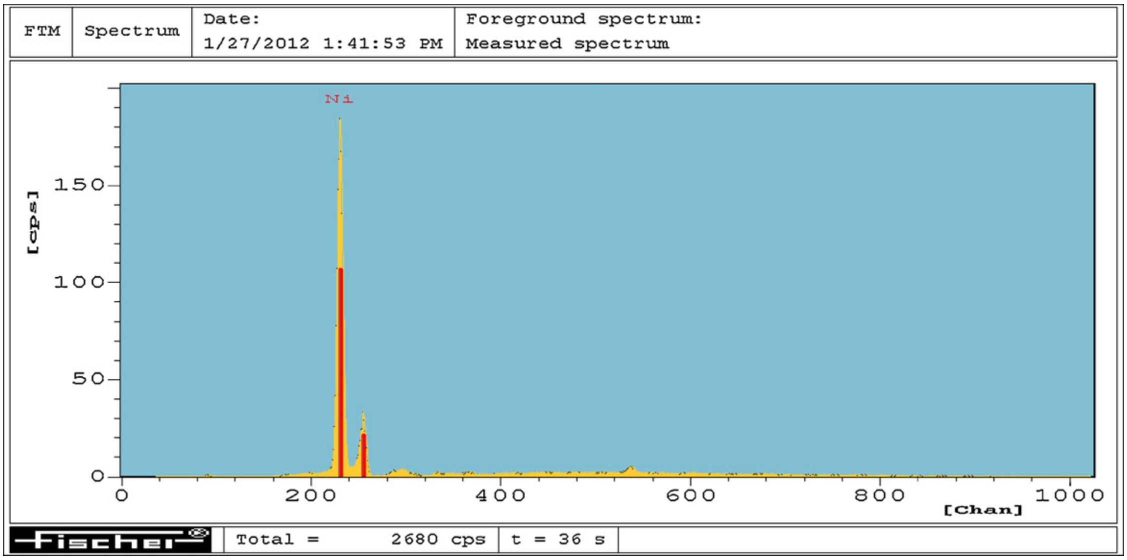

Fig. 4. ED-XRF spectrum of NiTSPc@APTES@SiO_2.

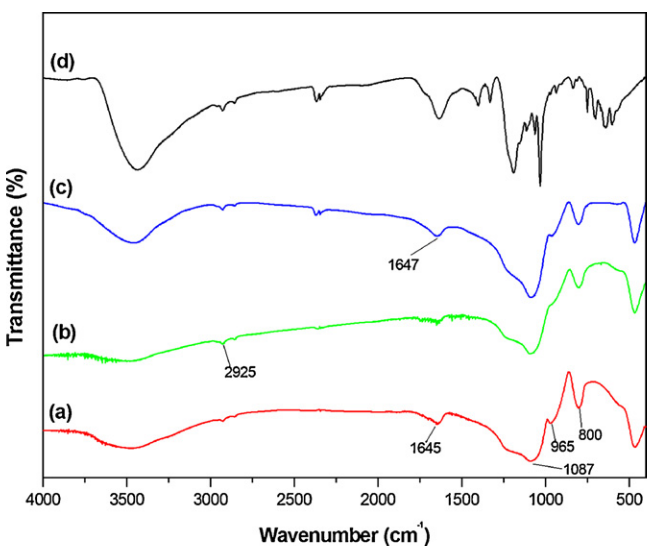

Fig. 5. FT-IR spectra of (a) SiO_2, (b) APTES@SiO_2, (c) NiTSPc@APTES@SiO_2 and (d) NiTSPc.

corresponding peak indicating a slight disorder in the APTES@SiO_2 and NiTSPc@APTES@SiO_2. The decreasing trend in the intensity can be accredited to the lowering of scattering contrast between the walls of the silica framework and organic/organometallic groups in the pores. Furthermore, no novel diffraction peak appeared even after the modification reactions which indicate that these species (APTES and NiTSPc) exist in the form of non-crystalline state on the surface of SiO_2.

Table 1
Physico-chemical parameters of SiO_2, APTES@SiO_2 and NiTSPc@APTES@SiO_2.

Material	Elemental analysis (weight %)			Surface area S_{BET} (m^2/g)
	C	H	N	
SiO_2	–	–	–	235
APTES@SiO_2	3.26	1.75	1.21	174
NiTSPc@APTES@SiO_2	19.08	4.98	5.18	141

3.2.7. Scanning electron microscopy

The morphology of NiTSPc@APTES@SiO_2 is characterized by Scanning electron microscopy. SEM micrographs are presented at two different magnifications. Apparently, the surface of bare SiO_2 is smooth (Fig. 7b) and become rough after the grafting of NiTSPc (Fig. 7d). Moreover, no clog between particles occurred during the preparation process, and the particles maintained regular lumpy shape (Fig. 7a and c). It could be seen that the particles appearance and size of these two samples are very similar, demonstrating that the particles of SiO_2 had good mechanical stability, and they had not been destroyed during the whole surface modification reaction.

3.3. Optimization of the reaction conditions

In industries, as cost often decides whether or not a particular protocol is chosen, the search for an efficient and cost-effective catalytic reaction conditions is highly desirable. Thus, we set out to optimize various reaction conditions: those that allow for maximum removal of dye using the less amounts of catalyst and oxidant, and those requisite for complete removal of dyestuffs in short duration of time.

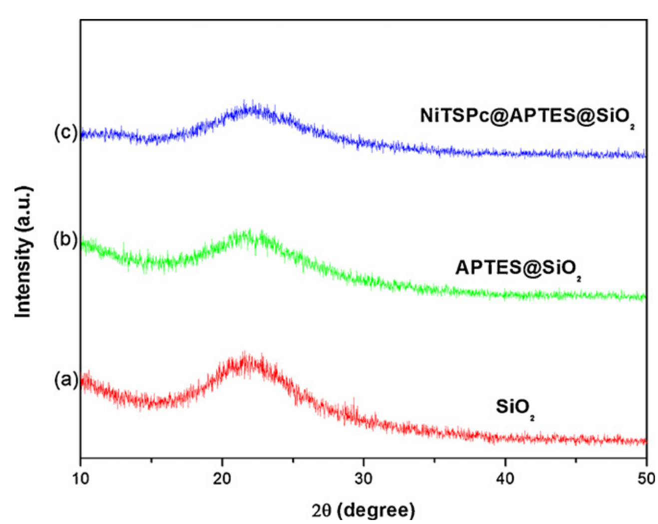

Fig. 6. XRD patterns of (a) SiO_2 (b) APTES@SiO_2 and (c) NiTSPc@APTES@SiO_2.

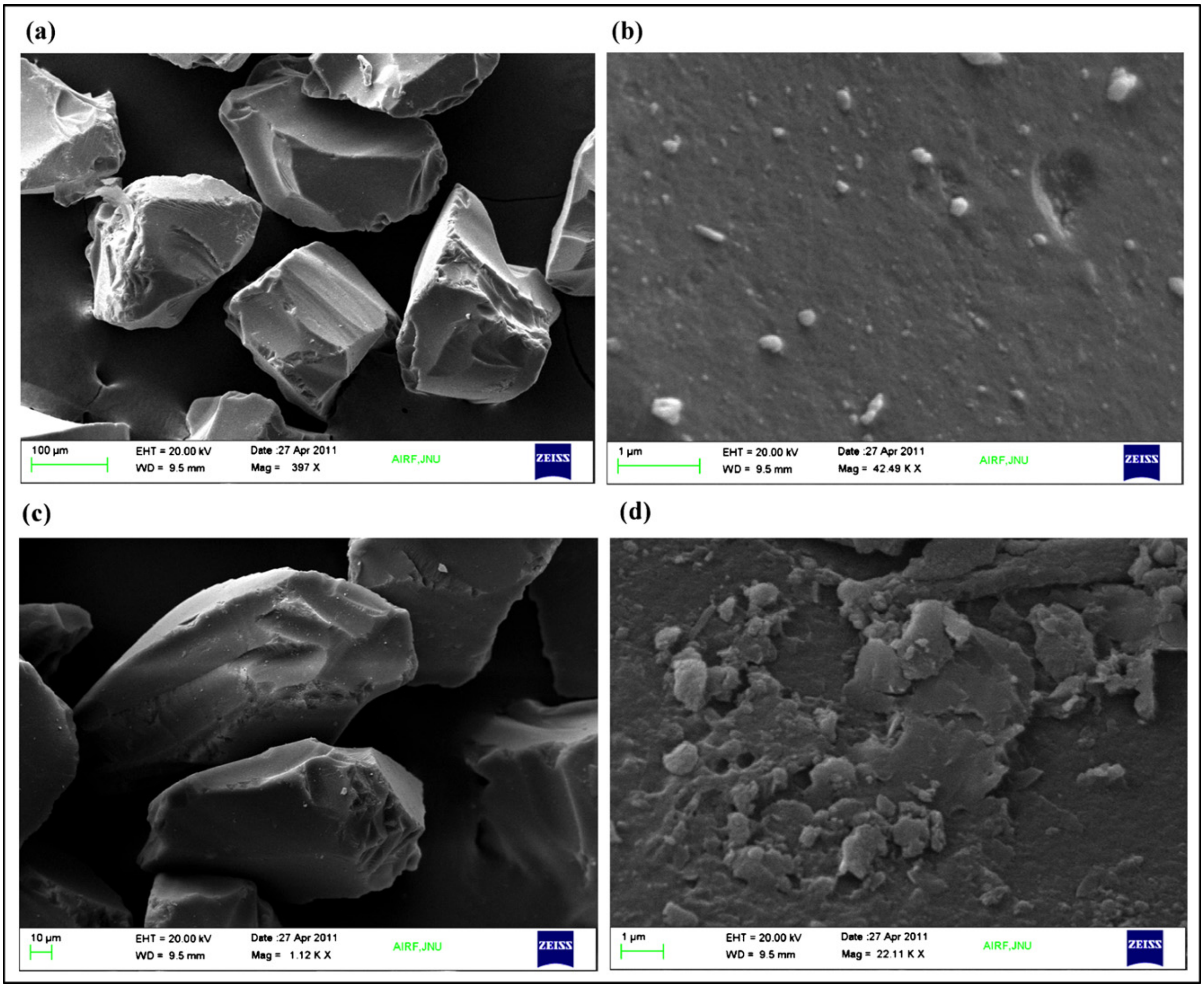

Fig. 7. SEM image of SiO_2 (a) at low magnification (b) at high magnification and NiTSPc@APTES@SiO_2 (c) at low magnification (d) at high magnification.

3.3.1. *Effect of H_2O_2 dosage*

The extent of degradation of dye (Methyl Orange) differs on varying the amount of H_2O_2 (30% wt% in water) used. As its dosage is associated exclusively with the absorbance at 462 nm thus, a decrease of the absorbance at 462 nm has been measured after several consecutive additions of known aliquots of H_2O_2 (Fig. 8). The influence of H_2O_2 dose on dye degradation was investigated at different concentrations (4–26 mmol, 2–3 mL) of hydrogen peroxide, while maintaining constant the quantity of catalyst used, dye concentration and pH. As expected, the increase in amount of hydrogen peroxide accelerated the degradation of Methyl Orange at the beginning of the reaction. But, when the hydrogen peroxide dose was increased from 17.6 to 26 mmol (2–3 mL), under same operation conditions, the degradation efficiency decreased. This could be due to the formation of hydroperoxyl radicals ($HO_2^{\bullet}$) in the presence of excess of H_2O_2.

$$H_2O_2 + OH^{\bullet} \rightarrow HO_2^{\bullet} + H_2O \qquad (1)$$

The hydroperoxyl radicals are much less reactive and do not contribute to the oxidative degradation of the organic substrate which takes place only through the reaction with $HO^{\bullet}$ [45]. It can be concluded that the H_2O_2 dose higher than 17.6 mmol (2 mL) corresponds to an unprofitable consumption of hydrogen peroxide. Thus, the effective dosage of H_2O_2 was fixed as 17 mmol (2 mL) for further studies.

3.3.2. *Effect of catalyst loading*

To investigate the effect of NiTSPc@APTES@SiO_2 loading on dye degradation, different catalyst loadings (0, 5, 10, 15, 20, 25 and

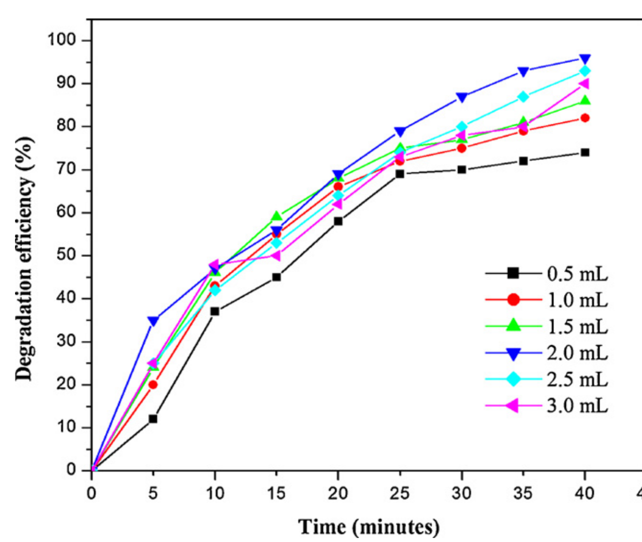

Fig. 8. Effect of H_2O_2 dosage on the catalytic degradation of Methyl Orange (pH 7.0, dye concentration = 10 mg/L, catalyst loading = 20 mg, room temperature = 27 °C).

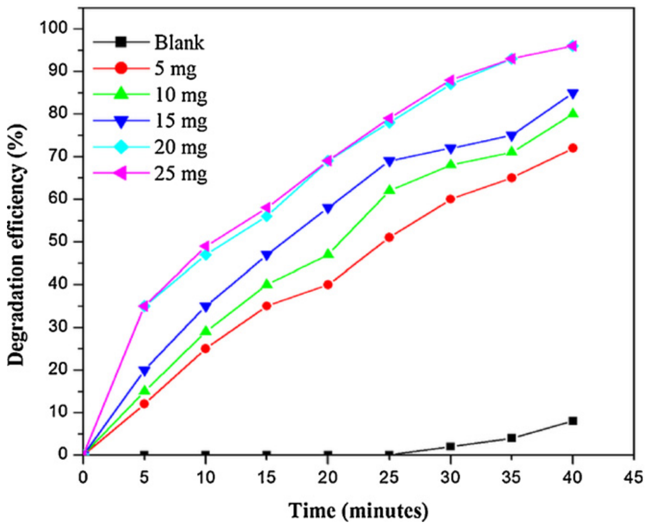

Fig. 9. Effect of catalyst loading on dye degradation, (reaction conditions: pH 7.0, dye concentration = 10 mg/L, 17.6 mmol H_2O_2, room temperature = 27 °C).

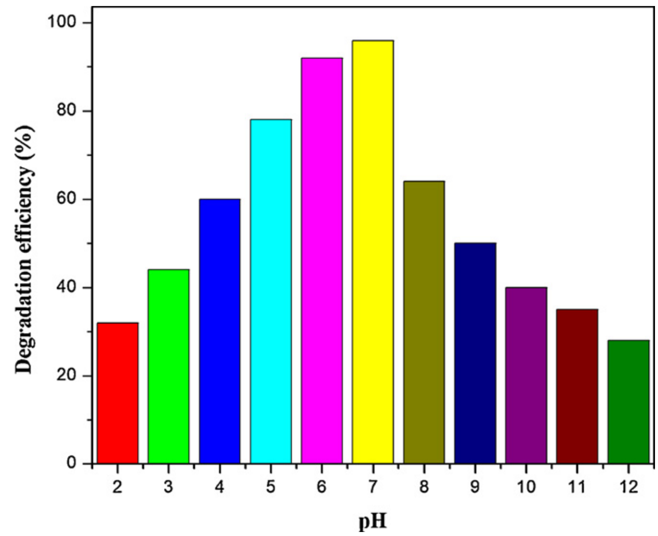

Fig. 10. Effect of pH on Degradation efficiency (reaction conditions: dye concentration = 10 mg/L, catalyst = 20 mg, 17.6 mmol H_2O_2, room temperature = 27 °C).

30 mg) were tested. Fig. 9 shows the results obtained for dye degradation as a function of time and catalyst loading. As can be seen from Fig. 9, the degradation efficiency without catalyst was very low with only 8% degradation after 40 min. Addition of only 5 mg catalyst in dye solution the degradation efficiency after 40 min reached at 72%, indicating that the catalyst was highly active. The degradation efficiency after 40 min reached 80, 85 and 96% when catalyst loading was 10, 15 and 20 mg respectively. It can be seen that with increasing concentration of the catalyst, there is decrease in the residual concentration of dye in the solution indicating increase in the degradation of dye. But, it is evident from Fig. 9 that above 20 mg, the removal of dye is not significantly higher. As the concentration of the catalyst was increased, the number of dye molecules adsorbed is increased owing to an increase in the number of silica particles. Above certain level, the dye molecules available are not sufficient for adsorption by the increased number of silica particles. Hence, the additional catalyst is not involved in the catalysis activity and the rate does not increase with an increase in the amount of catalyst beyond a certain limit. Further, for the catalyst concentration of 20 and 25 mg the amount of dye removed is the almost same (about 96%) after 45 min of treatment time. Hence, 20 mg has been taken as optimum catalyst concentration for further experiments.

3.3.3. Effect of pH

The solution pH significantly influences the degradation of organic dyes. There are several factors which influence the effect of pH on dye degradation. These include the surface area of the catalyst, nature of the dye and extent of the substrate adsorption on the catalyst surface. In this study the effect of pH were examined by adjusting the initial pH of dye solution in the range 2–12 for a period of 40 min. Fig. 10 shows the degradation percentage at various pH values. The dye is a fused polynuclear aromatic compound with an extensive π electron conjugation which can easily form a stable complex by donating electrons to the vacant d-orbital of the Nickel phthalocyanine. In other words, the Methyl Orange dye acts as a strong Lewis base and can easily adsorb on the catalyst surface. The degradation decreased by further lowering the pH value. This is because of the reason that at lower pH values, more H^+ is available for adsorption to mask the surface of the catalyst. On the other hand, degradation percentage was also less in basic media as compared to the neutral pH. This can be explained on the basis that at high pH values, OH ions will be preferably adsorbed on the catalyst surface thus reducing the overall efficiency of the catalyst. By keeping this knowledge, we have proceeded with degradation experiments of dye at pH 7. Also, a neutral pH condition is generally preferable because operation under neutral conditions can easily apply to most wastewater. On the other hand, acidic conditions significantly enhance the leaching of active component.

3.4. Evaluation of catalytic activity of NiTSPc@APTES@SiO_2

The catalytic activity of NiTSPc@APTES@SiO_2 was evaluated using the degradation of Methyl Orange under optimized reaction conditions. The dye degradation was carried out in a reaction flask containing 25 mL dye solution (10 mg/L), 2 mL H_2O_2 (17.6 mmol) and 20 mg catalyst. The reaction mixture was continuously shaked on a rotary shaker. The concentration of the dye in the reaction mixture was monitored by using a UV–vis spectrophotometer. The UV–vis spectrum of Methyl Orange consists of peak at 462 nm corresponding to the conjugated structure constructed via the azo group and aromatic rings in Methyl Orange molecules [46]. During the decolorization process, it was observed that the characteristic absorption peak (462 nm) decreased and almost disappeared during the course of the study (Fig. 11). This shows that the chromophore and conjugated system were being destroyed. For degradation studies, the λ_{max} of the dye (462 nm) was chosen for further investigations.

3.5. Kinetic studies

In order to study the kinetic control of dye adsorption on the catalyst, dye solution (3×10^{-5} M) was agitated in a rotary mechanical shaker with catalyst (0.02 g) in absence of H_2O_2 prior to degradation studies. The apparent kinetics of disappearance of the substrate Methyl Orange was determined by following the concentration of the substance at various time intervals using UV–vis spectrophotometer. It was observed that concentration of Methyl Orange decreased drastically during first 15 min and afterwards did not change considerably due to saturation of adsorption of Methyl Orange over the catalyst surface (Fig. 12). The concentration of Methyl Orange was decreased by 6% over NiTSPc@APTES@SiO_2 catalyst after 45 min due to adsorption.

For studying the reaction kinetics of dye degradation, a mixture of dye (3×10^{-5} M), NiTSPc@APTES@SiO_2 catalyst (0.02 g) and H_2O_2 (17.6 mmol, 2 mL) was agitated in a rotary mechanical shaker and the change in the electronic absorption spectra of

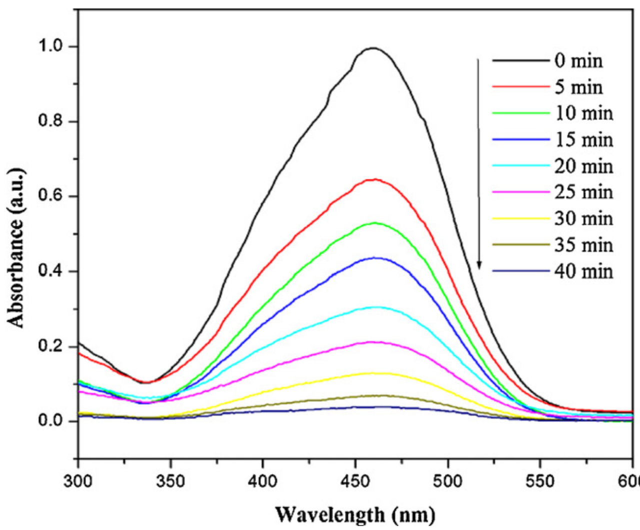

Fig. 11. Catalytic evaluation NiTSPc@APTES@SiO_2 for degradation of Methyl Orange (reaction conditions: dye concentration = 10 mg/L, pH 7, catalyst = 20 mg, 17.6 mmol H_2O_2, room temperature = 27 °C).

the dye solution was monitored at regular time intervals. It was noted that the absorbance value of the dye became less with time as shown in Fig. 11. The decrease in concentration value of dye solution can be related in terms of the degradation efficiency. The change in concentration value of the dye solution during its degradation was used to find out the reaction kinetics. The Methyl Orange degradation fitted best to the following pseudo first-order kinetic equation which is given by:

$$\ln\left(\frac{C_0}{C_t}\right) = k_{obs}t \tag{2}$$

where C_0 is the initial concentration of Methyl Orange, C_t is the concentration of Methyl Orange at time t, and k_{obs} is the observed reaction rate constant obtained from the slope of the line in the plot of $\ln(C_0/C_t)$ versus time. Fig. 13 shows the best fit of above Eq. (2) to the observed changes.

3.6. Catalyst stability and reusability

Reusability is one of the important advantages of a heterogeneous catalyst, which can also gives useful information about the immobilization process and catalytic stability along the catalytic cycles. To address the concern, a series of tests were undertaken. To test if the metal is leached out from the catalyst during the degradation reaction, the reaction mixture is collected by filtration. The absence of metal ions in the filtrate (Atomic absorption spectrometric analysis) demonstrates that Nickel does not leach out from the catalyst during oxidative degradation reaction, which is very important for its practical applications. After the catalytic reactions were completed, catalyst was recovered by filtration and washed with ethanol and dried in oven. It is evident from Fig. 14 that there was no obvious difference in the extent of degradation of Methyl Orange after 7 consecutive recycles of the catalyst.

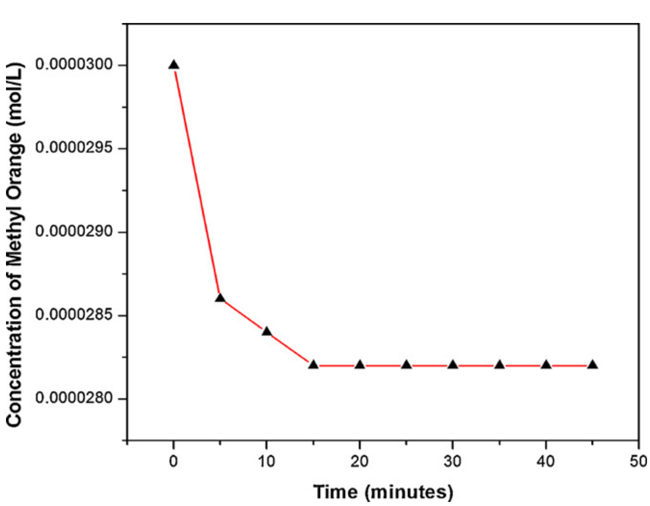

Fig. 12. Kinetics of dye adsorption on catalyst (reaction conditions: dye concentration = 10 mg/L, pH 7, catalyst = 20 mg, room temperature = 27 °C).

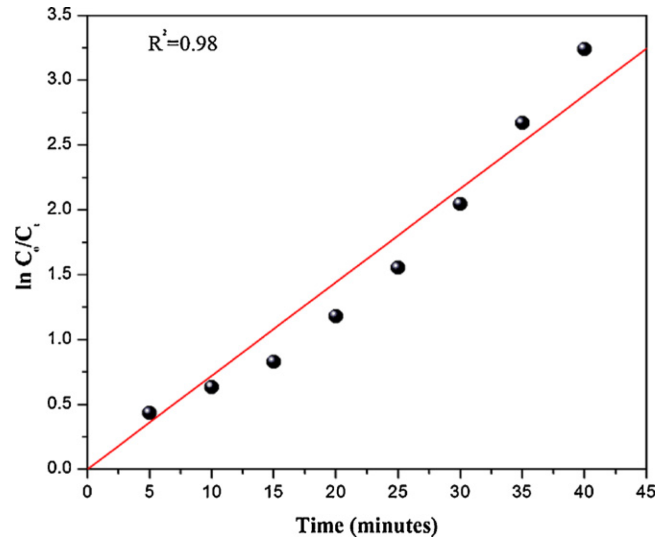

Fig. 13. Kinetic analysis of degradation of Methyl Orange under optimized conditions.

3.7. Plausible mechanism

The suggested mechanism claims that the catalyst activates the H_2O_2 molecules, leading to the formation of highly active oxidizing species hydroxyl radicals, $^{\bullet}OH$. The latter attacks the dyes forming an active intermediate (dye/radical adduct), which decomposed

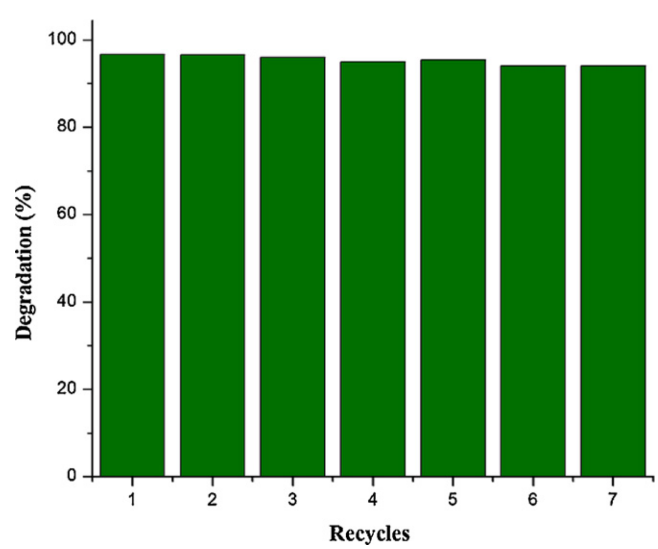

Fig. 14. Recyclability tests for NiTSPc@APTES@SiO_2 (reaction conditions: dye concentration = 10 mg/L, pH 7, catalyst = 20 mg, 17.6 mmol H_2O_2, room temperature = 27 °C).

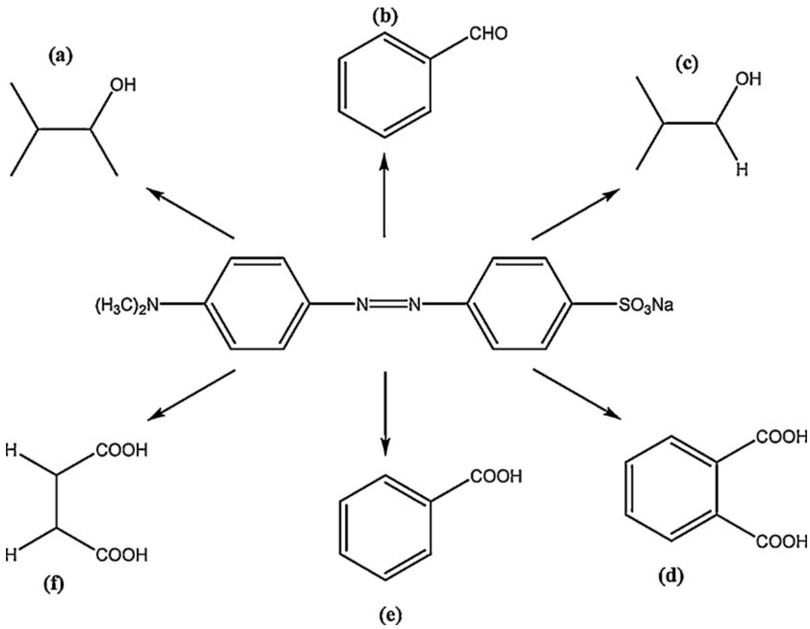

Fig. 15. Degradation products of Methyl Orange.

itself giving the final oxidation products, as shown in the following equations scheme:

$$Ni^{II}TSPc + H_2O_2 \rightarrow Ni^{III}TSPc + {}^{\bullet}OH + {}^{-}OH \quad (3)$$

$$^{\bullet}OH + Dye \rightarrow [Dye(^{\bullet}OH)] \quad (4)$$

$$[Dye(^{\bullet}OH)] \rightarrow Oxidized \quad products + CO_2 + H_2O \quad (5)$$

3.8. GC–MS studies for product analysis

The analysis of products formed after degradation experiment is very important for evaluating the overall success of catalytic processes because degradation products may negatively impact the environment and, the effects may be equal to or greater than those of the starting materials. Thus, Gas chromatography–mass spectrometry (GC–MS) was used to identify residual organic compounds in the reaction mixture. The results revealed that all the measurable oxidation products were mainly small

Table 2
Catalytic Degradation of azo dyes.[a]

Entry	Dye (Mol.wt./g mol^{-1})	Structure	λ_{max} (nm)	Time (min)	Degradation efficiency (%)
1	Methyl Red (269.3)	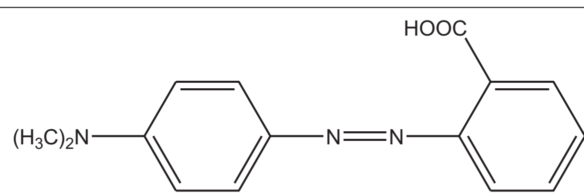	540	50	>95
2	Orange G (350.33)	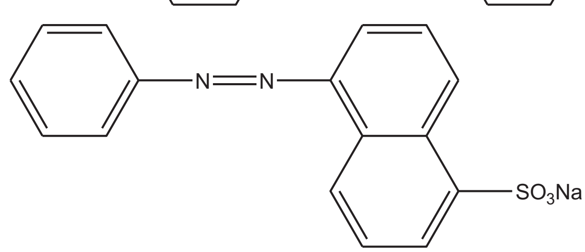	495	60	>96
3	Congo Red (696.68)	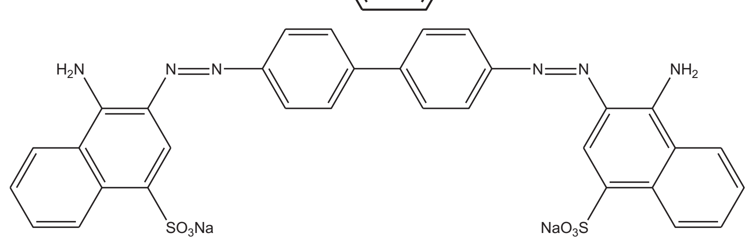	510	90	>93

[a] Reaction conditions: Dye (25 mL), Catalyst (20 mg), H_2O_2 (2 mL), room temperature.

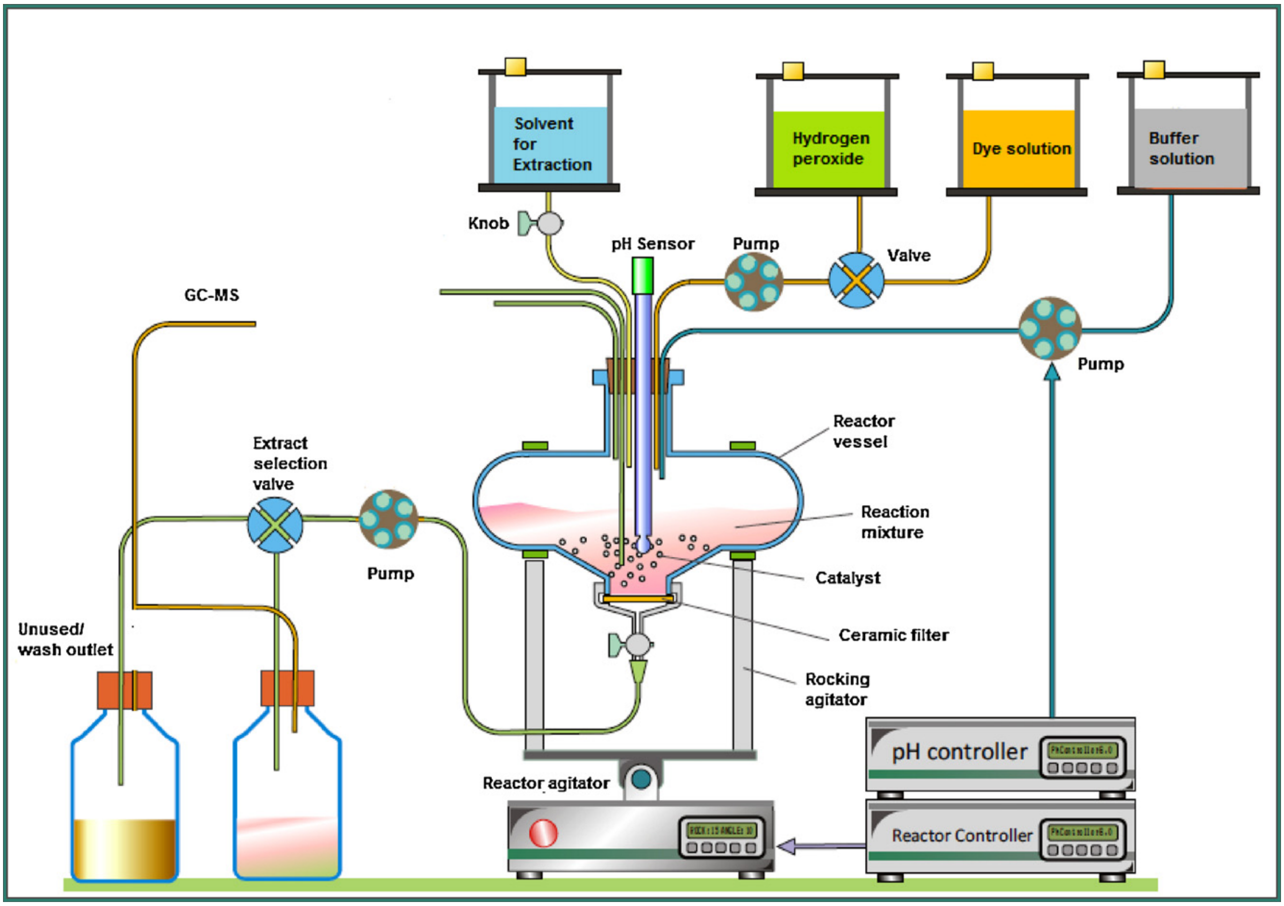

Fig. 16. Schematic illustration of the reactor system.

organic molecules (Fig. 15), which are known to be biologically degradable.

3.9. Degradation of other dyes

One of the most significant factors for the evaluation of a novel catalytic system is the scope of substrates. The most important requisite for effective catalysts that degrade dye pollutants is that the catalyst is able to degrade a wide range of dye pollutants. It is evident from Table 2 that under optimized degradation conditions the present catalytic system NiTSPc@APTES@SiO_2 show high degradation efficiency for several other azo dyes also.

3.10. Large scale degradation in a newly designed reactor

A novel batch mode chemical reactor with automation has been designed [47] for the first time which opens up a new avenue for the effective and large scale degradation of dyes at room temperature using recyclable organic–inorganic hybrid catalyst, NiTSPc@APTES@SiO_2. The reactor consists of the following units: (i) Batch reactor with a volume capacity of 5–10 L fitted with an agitator, (ii) pH adjusting unit consisting of a pH controller with a probe electrode and buffer solution chambers, and (iii) Oxidant unit containing suction pump attached to the reactor through polypropylene tube in order to pump out the oxidizing agent (160 mL) from it at a controlled flow rate (Fig. 16). Initially, the batch reactor was charged with an optimized amount of silica supported catalyst (1.6 g), and then the dye solution (2 L) was poured into it through an inlet tube. The pH of the solution was adjusted to required value with the help of pH adjusting unit, and thereafter the mixture in the reactor was subjected to agitation continuously so as to maintain a homogeneous environment. Samples were withdrawn from the reaction vessel at regular time intervals through a polypropylene tube at the bottom of the reactor and the concentration of dye solution was determined directly using UV–visible spectrophotometer. The degradation efficiency was found in good

Table 3
Literature precedents for the degradation of Methyl Orange.

Entry	Catalyst	Reaction conditions	Time (min)	Degradation efficiency (%)	Ref.
1	Fe_2O_3-CeO_2-TiO_2/γ-Al_2O_3	Atmospheric pressure, air oxidation (400 ml min^{-1})	150	98.09	[48]
2	Fe_2O_3/SiO_2	H_2O_2, initial pH 2.93, 100 °C	20	90	[49]
3	Cu(II)-polyampholyte/system	H_2O_2, pH 7.0, room temperature	20	90	[50]
4	α-Fe2O3-supported HY zeolite	pH 2, fluorescent lamp (20 W) light source	120	80	[51]
5	Pt-TiO_2/zeolites	UV light source, H_2O_2, calcinated at 200 °C	30	86.2	[52]
6	Yttrium incorporated TiO_2 supported ZSM-5	Photon flux of 4.7×10^{15} photons/s	240	97.3	[53]
7	Poly(3-hexylthiophene)-modified TiO_2	Visible light (300 W iodine tungsten lamp)	600	88.5	[54]
8	$H_3PW_{12}O_{40}$ supported Fe-bentonite	H_2O_2, 30 °C, UV light	60	90	[55]
9	Zirconia nanotubes	Ultrasonic wave, pH 2	480	97.6	[56]

agreement with the earlier determined value using rotary mechanical shaker on smaller scale. After the reaction, the catalyst was washed, dried and recycled for next run.

3.11. Comparison of the prepared catalytic system with the literature precedents

Table 3 represents the literature precedents [48–56] of various catalytic systems for degradation of Methyl Orange, and their degradation efficiencies have been compared with those obtained by using NiTSPc@APTES@SiO_2 catalyst. It is evident from the comparison of the results obtained that degradation efficiency of the present catalytic system is remarkable making it superior to some reported catalysts in terms of mild reaction conditions, short degradation time, easy work-up, and easy recovery and reusability of the catalyst renders the present protocol highly indispensable to address the industrial prerequisites and environmental concerns.

4. Conclusion

In conclusion, we have reported an environmentally benign method for oxidative degradation of azo dyes by H_2O_2 at room temperature using silica supported Nickel phthalocyanine catalyst, NiTSPc@APTES@SiO_2. The most important factors influencing the catalytic degradation of azo dyes were the catalyst loading, H_2O_2 dosage and pH. The additional advantages of this method include simplicity, economic viability, easy recovery and recyclability of the catalyst, and no metal sludge formation unlike the other known homogeneous catalytic methods. The utilization of automated batch reactor for the first time clearly demonstrates the considerable potential of this system for an effective degradation of organic pollutants in large scale at room temperature.

Acknowledgment

The financial assistance from University Grant Commission (UGC) and Department of Science and Technology (DST) under DU-DST PURSE grant is acknowledged. Due thanks to AIRF, JNU, Delhi, India for SEM analysis and IISc, Bangalore, India for solid state NMR measurements.

Appendix A. Supplementary data

Supplementary data associated with this article can be found, in the online version, at http://dx.doi.org/10.1016/j.apcatb.2012.05.046.

References

[1] C. O'Neill, R.F. Hawkes, D.L. Hawkes, N.D. Lourenco, H.M. Pinheiro, W. Delee, Journal of Chemical Technology and Biotechnology 74 (1999) 1009–1018.
[2] H. Kyung, J. Lee, W. Choi, Environmental Science and Technology 39 (2005) 2376–2382.
[3] P. Grau, Water Science and Technology 24 (1991) 97–103.
[4] M.H.M. Pinheiro, E. Touraud, O. Thomas, Dyes and Pigments 61 (2004) 121–139.
[5] J.M. Peralta-Hernandez, C.A. Martinez-Huitle, J.L. Guzman-Mar, A. Hernandez-Ramirez, Journal of Environmental Engineering Management 19 (2009) 257–265.
[6] M.F. Variava, T.L. Church, A.T. Harris, Applied Catalysis B: Environmental 123–124 (2012) 200–207.
[7] W.J. Eilbeck, G. Mattock, Chemical Processes In Wastewater Treatment, Ellis Horwood Ltd, 1987.
[8] W. Stumm, J.J. Morgan, American Water Works Association (1962) 971–992.
[9] G. Tchobanoglous, F.L. Burton, Wastewater Engineering, McGraw-Hill Inc, 1991.
[10] S.K. Bhattacharya, Treatment of textile wastes, in: L.K. Wang, M.H.S. Wang (Eds.), Handbook of Industrial Waste Treatment, 1, New York, 1992.
[11] R. Andreozzi, V. Caprio, A. Insola, R. Marotta, Catalysis Today 53 (1999) 51–59.
[12] M.P. Titus, V.G. Molina, M.A. Banos, J. Gimenez, S. Esplugas, Applied Catalysis B: Environmental 47 (2004) 219–256.
[13] W. Lu, W. Chen, N. Li, M. Xu, Y. Yao, Applied Catalysis B: Environmental 87 (2009) 146–151.
[14] B. Agboola, K. Ozoemena, T. Nyokong, Journal of Molecular Catalysis A: Chemical 227 (2005) 209–216.
[15] A. Sun, Z.G. Xiong, Y.M. Xu, Journal of Molecular Catalysis A: Chemical 259 (2006) 1–6.
[16] W. Xu, H. Guo, D.L. Akins, Journal of Physical Chemistry B 105 (2001) 1543–1546.
[17] Z. Xiong, Y. Xu, Chemistry of Materials 19 (2007) 1452–1458.
[18] W.J. DeSisto, R. Cashon, D. Cassidy, N. Hill, D.M. Ruthven, J.B. Paine III, J.A. Fournier, Industrial & Engineering Chemistry Research 47 (2008) 7857–7861.
[19] C.S. Shen, S.F. Song, L.L. Zang, X.D. Kang, Y.Z. Wen, W.P. Liu, L.S. Fu, Journal of Hazardous Materials 177 (2010) 560–566.
[20] R. Sharma, S. Dhingra Designing and Synthesis of Functionalized Silica Gels and their Applications as Metal Scavengers, Sensors, and Catalysts: A Green Chemistry Approach, LAP Lambert Academic Publishing LAP Lambert Academic Publishing, Germany, 2011.
[21] R.K. Sharma, C. Sharma, Tetrahedron Letters 51 (2010) 4415–4418.
[22] R.K. Sharma, D. Rawat, Journal of Inorganic and Organometallic Polymers 21 (2011) 619–626.
[23] R.K. Sharma, C. Sharma, Catalysis Communications 12 (2011) 327–331.
[24] R.K. Sharma, D. Rawat, G. Gaba, Catalysis Communications 19 (2012) 31–36.
[25] R.K. Sharma, D. Rawat, Inorganic Chemistry Communications 17 (2012) 58–63.
[26] R.K. Sharma, A. Goel, Analytica Chimica Acta 534 (2005) 137–142.
[27] R.K. Sharma, C. Sharma, Journal of Molecular Catalysis A: Chemical 332 (2010) 53–58.
[28] R.K. Sharma, A. Pandey, S. Gulati, A. Adholeya, Journal of Hazardous Materials 209-210 (2012) 285–292.
[29] A.M. Donia, A.A. Atia, W.A. Al-amrani, A.M. El-Nahas, Journal of Hazardous Materials 161 (2009) 1544–1550.
[30] P.J. Camp, A.C. Jones, R.K. Neely, N.M. Speirs, Journal of Physical Chemistry A 106 (2002) 10725–10732.
[31] X.B. Leng, C.F. Choi, H.B. Luo, Y.K. Cheng, D.K.P. Ng, Organic Letters 9 (2007) 2497–2500.
[32] A.R. McDonald, N. Franssen, G.P.M.V. Klink, G.V. Koten, Journal of Organometallic Chemistry 694 (2009) 2153–2162.
[33] S.B. Hartono, S.Z. Qiao, J. Liu, K. Jack, B.P. Ladewig, Z. Hao, G.Q.M. Lu, Journal of Physical Chemistry C 114 (2010) 8353–8362.
[34] E. DeOliveira, C.R. Neri, A.O. Ribeiro, V.S. Garcia, L.L. Costa, A.O. Moura, A.G.S. Prado, O.A. Serra, Y. Iamamoto, Journal of Colloid and Interface Science 323 (2008) 98–104.
[35] S. Shylesh, A.P. Singh, Journal of Catalysis 244 (2006) 52–64.
[36] R. Kureshy, I. Ahmad, N.H. Khan, S. Abdi, S. Singh, P. Pandia, R. Jasra, Journal of Catalysis 235 (2005) 28–34.
[37] S. Shylesh, A.P. Singh, Journal of Catalysis 228 (2004) 333–346.
[38] A. Bhatt, K. Pathak, R. Jasra, R. Kureshy, N. Khan, S. Abdi, Journal of Molecular Catalysis A: Chemical 244 (2005) 110–117.
[39] D.J. Upadhyaya, S.D. Samant, Applied Catalysis A: General 340 (2008) 42–51.
[40] C. Pereira, S. Patricio, A.R. Silva, A.L. Magalhaes, A.P. Carvalho, J. Pires, C. Freire, Journal of Colloid and Interface Science 316 (2007) 570–579.
[41] A.B. Sorokin, A. Tuel, Catalysis Today 57 (2000) 45–59.
[42] H.F. Hoefnagels, D. Wu, G. de With, W. Ming, Langmuir 23 (2007) 13158–13163.
[43] J.-L. Liu, S. Xu, B. Yan, Colloids and Surfaces A: Physicochemical and Engineering Aspects 373 (2011) 116.
[44] M. Kruk, M. Jaroniec, Y. Sakamoto, O. Terasaki, R. Ryoo, C.H. Ko, Journal of Physical Chemistry B 104 (2000) 292–301.
[45] N.N. Fathima, R. Aravindhan, J.R. Rao, B.U. Nair, Chemosphere 70 (2008) 1146–1151.
[46] Z. Mesgari, M. Gharagozlou, A. Khosravi, K. Gharanjig, Applied Catalysis A: General 411–412 (2012) 139–145.
[47] A. Adholeya, R.K Sharma, Patent: CBR 4171146/del/2010.
[48] Y. Liu, D. Sun, Applied Catalysis B: Environmental 72 (2007) 205–211.
[49] N. Panda, H. Sahoo, S. Mohapatra, Journal of Hazardous Materials 185 (2011) 359–365.
[50] J.M.L. Martinez, M.F.L. Denis, L.L. Piehl, E.R. de Celis, G.Y. Buldain, V.C. Dall' Orto, Applied Catalysis B: Environmental 82 (2008) 273–283.
[51] N.F. Jaafar, A.A. Jalil, S. Triwahyono, M.N.M. Muhid, N. Sapawe, M.A.H. Satar, H. Asaari, Chemical Engineering Journal (2012), http://dx.doi.org/10.1016/j.cej.2012.02.077.
[52] M. Huang, C. Xu, Z. Wu, Y. Huang, J. Lin, J. Wu, Dyes and Pigments 77 (2008) 327–334.
[53] A.N. Okte, O. Yilmaz, Applied Catalysis B: Environmental 85 (2008) 92–102.
[54] D. Wang, J. Zhang, Q. Luo, X. Li, Y. Duaa, J. An, Journal of Hazardous Materials 169 (2009) 546–550.
[55] G. Wei, C. Fan, L. Zhang, R. Ye, T. Wei, Z. Tong, Catalysis Communications 17 (2012) 184–188.
[56] J. Zhao, X. Wang, L. Zhang, X. Hou, Y. Li, C. Tang, Journal of Hazardous Materials 188 (2011) 231–234.